The Journal of Experimental Biology 204, 1547–1557 (2001)
Printed in Great Britain © The Company of Biologists Limited 2001
JEB3248

HYDRODYNAMIC DRAG OF DIVING BIRDS: EFFECTS OF BODY SIZE, BODY SHAPE AND FEATHERS AT STEADY SPEEDS

JAMES R. LOVVORN[1,*], GEOFFREY A. LIGGINS[2,‡], MATTHIAS H. BORSTAD[2], SANDER M. CALISAL[2] AND JON MIKKELSEN[2]

[1]*Department of Zoology, University of Wyoming, Laramie, WY 82071, USA* and [2]*Department of Mechanical Engineering, University of British Columbia, Vancouver, British Columbia, Canada V6T 1Z4*

*e-mail: lovvorn@uwyo.edu

‡Present address: C-CORE, Memorial University of Newfoundland, St John's, Newfoundland, Canada A1B 3X5

Accepted 7 February; published on WWW 5 April 2001

Summary

For birds diving to depths where pressure has mostly reduced the buoyancy of air spaces, hydrodynamic drag is the main mechanical cost of steady swimming. Drag is strongly affected by body size and shape, so such differences among species should affect energy costs. Because flow around the body is complicated by the roughness and vibration of feathers, feathers must be considered in evaluating the effects of size and shape on drag. We investigated the effects of size, shape and feathers on the drag of avian divers ranging from wing-propelled auklets weighing 75 g to foot-propelled eiders weighing up to 2060 g. Laser scanning of body surfaces yielded digitized shapes that were averaged over several specimens per species and then used by a milling machine to cut foam models. These models were fitted with casts of the bill area, and their drag was compared with that of frozen specimens. Because of the roughness and vibration of the feathers, the drag of the frozen birds was 2–6 times that of the models. Plots of drag coefficient (C_D) *versus* Reynolds number (*Re*) differed between the model and the frozen birds, with the pattern of difference varying with body shape. Thus, the drag of cast models or similar featherless shapes can differ both quantitatively and qualitatively from that of real birds. On the basis of a new towing method with no posts or stings that alter flow or angles of attack, the dimensionless C_D/*Re* curves differed among a size gradient of five auklet species (75–100 g) with similar shapes. Thus, extrapolation of C_D/*Re* curves among related species must be performed with caution. At lower speeds, the C_D at a given *Re* was generally higher for long-necked birds that swim with their neck extended (cormorants, grebes, some ducks) than for birds that swim with their head retracted (penguins, alcids), but this trend was reversed at high speeds. Because swimming birds actually travel at a range of instantaneous speeds during oscillatory strokes, species variations in drag at different speeds must be considered in the context of accelerational stroking.

Key words: cost of diving, diving, bird, drag, swimming, feather, laser scanning, model fabrication, shape effects.

Introduction

Fluid mechanical drag is critical to the energy costs of flight and diving in birds and mammals (Kooyman, 1989; Pennycuick, 1989; Lovvorn et al., 1991; Lovvorn et al., 1999). At depths where pressure has substantially reduced the volume and buoyancy of air in the respiratory system and plumage, drag becomes the main mechanical cost of steady swimming (Lovvorn, 2001). Body size has strong effects on drag because it determines the ratio of mass to surface area and, thus, the ratio of inertial to viscous (friction) forces. Body shape also has an important influence on drag by altering the point along the body where boundary-layer flow shifts from laminar to turbulent and the point where the boundary layer separates from the body (Hoerner, 1965; Webb, 1975; Aleyev, 1977). These points are further affected by the roughness and flexibility of the body surface, which can delay separation by inducing fully turbulent but attached flow (Aleyev, 1977) or enhance separation by surface flutter (Tucker, 1990; Pennycuick et al., 1996). We investigated the effects on drag of the size, shape and speed of diving birds and how these relationships are modified by the surface effects of the plumage.

Drag has been calculated from films of deceleration during gliding by live animals (Clark and Bemis, 1979; Bilo and Nachtigall, 1980; Feldkamp, 1987; Skrovan et al., 1999; Stelle et al., 2000). Deceleration measurements avoid problems with unnatural flutter of fur or feathers on dead specimens and are best for estimates of drag during gliding. However, deceleration values include the drag of propulsive limbs and are at much lower speeds than those achieved instantaneously during accelerational stroking. Thus, they are less satisfactory for modeling the drag of the body fuselage (head and trunk only) throughout strokes when the efficiency (including drag)

of propulsors is considered separately (Hui, 1988; Lovvorn et al., 1991; Lovvorn et al., 1999).

Drag has also been measured directly as the force needed to pull animals through a fluid. Live seals have been trained to cooperate in being towed behind moving carriages (Williams and Kooyman, 1985), but this approach has not been possible with less trainable birds. In most cases, drag measurements in flumes or behind carriages have been made on frozen specimens (Williams, 1983; Williams, 1989; Fish, 1984; Pennycuick et al., 1988; Tucker, 1990; Lovvorn et al., 1991; Lovvorn et al., 1999) or cast models (Purves et al., 1975; Aleyev, 1977; Hui, 1988; Oehme and Bannasch, 1989; Bannasch, 1993; Bannasch, 1995). With frozen specimens, obtaining sometimes rare species from distant or poorly accessible sites can be difficult, and the animals often become damaged or misshapen while dying or in storage. Also, frozen specimens thaw during repeated drag measurements in water and must be refrozen intermittently during trials. Cast models avoid the latter problem, but their rigid surfaces do not duplicate the effects of a flexible, vibrating pelage (Tucker, 1990; Pennycuick et al., 1996).

A method known as laser striping (Faugeras, 1996), in which three-dimensional surfaces are digitized as input for computer-driven carving machines, yields the advantages of cast models as well as allowing sampling among specimens. Digitized surfaces of various individuals can be scaled to the same mean length and averaged at all points on a standardized surface grid to yield an average shape. This digitization method can also generate scale models of very different sizes for the same species. The latter option is quite useful if the size or maximum speed of the flume or carriage, or the sensitivity of the measurement system, requires the use of different sizes or speeds of objects at the same Reynolds numbers. Nevertheless, as with cast models, this method does not consider the surface effects of flexible fur or feathers.

Because of the difficulty of obtaining frozen specimens and measuring the drag of all species of interest, it is often helpful to express the drag of particular shapes at different speeds in terms of non-dimensional variables: the drag coefficient (C_D) for drag scaled to surface area, and the Reynolds number (*Re*) for speed scaled to body length. A given shape will fall on the same curve of C_D *versus Re* regardless of its size or speed. If the shapes of two species are similar enough, then their C_D/*Re* curves should be the same irrespective of differences in size, implying that measurements are needed for only one of the species (e.g. Bannasch, 1995). However, the effects of slight variations in shape have seldom been evaluated as a source of potential error in extrapolating among species.

In this paper, we describe a method for fabricating models of animal shapes by laser striping, averaging of digitized surfaces and computer-driven machine carving. We compare the hydrodynamic drag of the resulting models with the drag of frozen birds used to develop the models, allowing us to examine interactions between body shape and feather effects. For frozen specimens, we also evaluate the similarity between C_D/*Re* curves for a size gradient of similar species (auklets), and compare the drag and C_D/*Re* patterns for a wide range of species of different sizes, shapes and swimming modes. Because the shapes and flow regimes of birds can change during complex maneuvers to pursue prey (see Spring, 1971), our measurements are relevant mainly to sustained, steady swimming such as when birds are traveling directly to and from the depth of foraging (Lovvorn et al., 1999; J. R. Lovvorn, A. Kato, Y. Watanuki and Y. Naito, unpublished results).

Materials and methods

Creation and preparation of bird models

Four to six individuals of each bird species were frozen in a diving posture. To measure the drag of the body fuselage (the head and body trunk without the propulsive limbs), the feet of foot-propelled divers and the wings of wing-propelled divers were removed. Thus, the measurements reported here do not account for the drag of propulsive limbs. In the modeling approach for which these measurements were made (see Lovvorn et al., 1991; Lovvorn et al., 1999; Lovvorn, 2001), the drag of oscillating propulsors is subsumed by the aerobic efficiency (mechanical power output/aerobic power input). This coefficient is used to calculate aerobic energy requirements from estimates of the mechanical power needed to propel the body fuselage at quasi-steady speeds. This approach is analogous to that often used in naval engineering, in which the drag of a hull is matched with a propulsive system of given net efficiency. In our case, this method obviates the need to measure the instantaneous drag of oscillating, rotating limbs throughout a quasi-steady stroke cycle, which no one has yet accomplished.

Surface areas were measured by taping polyethylene film snugly around the body without compressing the plumage, tracing the removed film on paper, and then weighing the traced sections of paper (Lovvorn et al., 1991). Partially thawed specimens were then mounted on sharpened steel rods (6.4 mm in diameter) inserted from the posterior end of the bird through the neck and into the head. After mounting, each specimen was refrozen in the posture for straight underwater swimming, as indicated by observations and photographs of birds in tanks.

The rod extending rearward from the mounted bird was inserted vertically into a chuck in a rotary indexing table, which allowed angular rotation of the bird by known increments around the rod axis. A laser instrument (35 mW, helium–neon red laser; Spectra-Physics Stabilite model 124B) was mounted along with the indexing table on an aluminum frame (Fig. 1). A cylindrical mirror 2 cm in diameter was mounted near the laser aperture in the path of the beam and reflected a vertical plane of light onto the axis of rotation of the mounted bird. The vertical plane of light was further focused by passing it through a long, vertical slot in a strip of paper hung in front of the bird. The result was an intense band of light a few millimeters wide that illuminated the profile of the bird in the plane of its angle of rotation (Fig. 1).

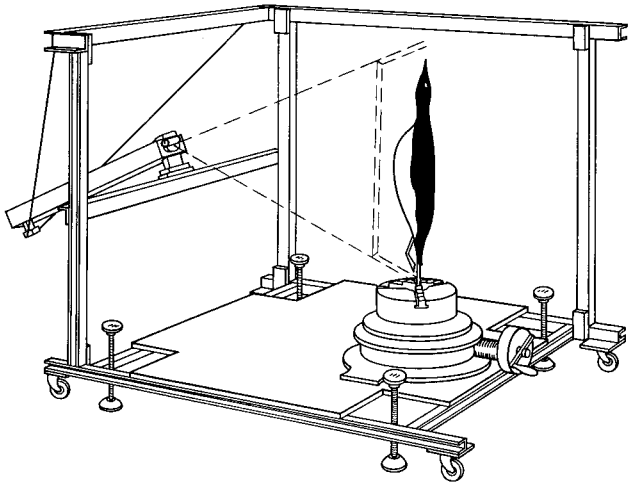

Fig. 1. Apparatus for illuminating the profile of a frozen bird using a thin laser sheet. The intensely illuminated profile was filmed with a video camera, recorded with a frame-grabber and then digitized. The bird was rotated through angular intervals for successive video images of the entire shape.

Approximately 3.5 m away from the frozen bird, at an angle to the plane of the laser beam, we mounted a Pulnix TM-20 video camera with an 8.5 mm charge coupled device (CCD) head and a 12 mm, 1:1.2 lens. Video images were recorded for 10 s at each 10 ° angular rotation of the indexing table. One image frame from each 10 s period was chosen for analysis. The profile of the bird from each angular perspective, defined by the intensely illuminated laser stripe in the video image frame, was digitized with a frame-grabber. The camera distance and its angle relative to the plane of the laser beam were used to transform the obtuse image to planar coordinates (Fu et al., 1987). The conical geometry of the camera's vision was then converted to flat geometry in the plane of the laser sheet to define the data in scaled polar coordinates. An ASCII file was created that contained both Cartesian and cylindrical (radius, height, radial angle) data. These data could be read by a variety of software packages, including software that we developed for averaging the digitized bird surfaces.

The digitized shape consisted of 200 transverse (cross-sectional) planes from the anterior to the posterior end of each bird, with the bird's surface on each plane defined by 72 radii projecting from the long axis of the animal. Corresponding radial lines from each side of the bird were averaged, resulting in 14 400 points defining the surface of the symmetrical, smoothed animal. The bird geometries were standardized by the lengths of respective individuals and then averaged among 4–6 individuals. Asymmetries resulting from damaged or otherwise misshapen parts of different specimens were deleted or subsumed by the average. The final output included a computer numerical control (CNC) toolpath file in the format specified by the milling machine.

Bird models were carved by the Vorum Research Corporation (Vancouver, British Columbia, Canada) with a CANFIT-PLUS milling machine designed for manufacturing

Fig. 2. Stages in the construction of the model for common guillemots, including (left to right) a frozen bird, the digitized shape averaged for five individuals, the foam carving and the finished model fitted with a cast of the bill area.

prosthetic limbs. The models were made of high-density urethane foam, with a hole 2.5 cm in diameter through the axis of the block. The neck of some species was less than 2.5 cm wide and could not be machined; these were later carved by hand. To reproduce the bill area for each model bird, molds and plaster casts were prepared from a selected individual of each species. The cast bill and face were cut and sanded to blend smoothly into the head of the foam model and waterproofed with epoxy resin. To fill cavities and create a smooth waterproof surface on the open-cell foam, a coat of 12 h epoxy resin mixed with lightweight filler (to improve sanding properties) was applied to each model (400 Microlight Fairing Filler, Gougeon Brothers, Inc., Bay City, Michigan, USA). After the epoxy resin had cured, the models were thoroughly sanded, and the process was repeated before painting. Stages in the construction of a bird model are shown in Fig. 2 and profiles of all models in Fig. 3.

The bird models were balanced and ballasted to neutral buoyancy at the depth of the experiments by inserting lead shot into the cylindrical cavity (2.5 cm wide) that passed through the axis of each model. The rear of the cavity was then plugged and smoothed with Plasticene. The surface areas of these models were measured by the same method used for frozen birds (see above). The dimensions of the models (Table 1) all fell within the ranges for the frozen birds used to develop the models.

Preparation of frozen birds

Single frozen specimens of each species, including specimens used to develop the models, were used for drag measurements (Table 2). To determine the drag of the body

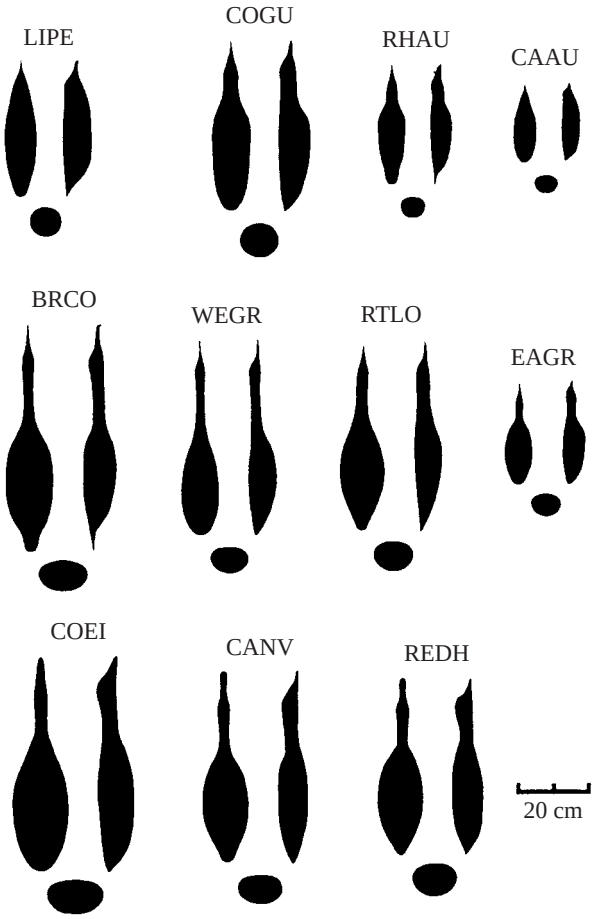

Fig. 3. Top (left), side (right) and frontal (bottom) profiles of bird models. Species codes are given in Table 1. Swimming-foraging types include wing-propelled penguins that do not fly in air (LIPE), wing-propelled alcids that also fly in air (COGU, RHAU, CAAU), foot-propelled pursuers (BRCO, WEGR, RTLO, EAGR) and foot-propelled benthivores (COEI, CANV, REDH).

Table 1. *Body length including the bill and tail (L_b), body wetted surface area (A_{sw}) and maximum frontal area of bird models*

Species	Species code	Length (m)	Surface area (m^2)	Frontal area (m^2)
Little penguin (*Eudyptula minor*)	LIPE	0.379	0.0686	0.0055
Common guillemot (*Uria aalge*)	COGU	0.478	0.0951	0.0076
Rhinoceros auklet (*Cerorhinca monocerata*)	RHAU	0.332	0.0474	0.0042
Cassin's auklet (*Ptychoramphus aleuticus*)	CAAU	0.220	0.0318	0.0029
Brandt's cormorant (*Phalacrocorax penicillatus*)	BRCO	0.632	0.1139	0.0096
Red-throated loon (*Gavia stellata*)	RTLO	0.508	0.0882	0.0083
Western grebe (*Aechmophorus occidentalis*)	WEGR	0.558	0.0838	0.0066
Eared grebe (*Podiceps auritus*)	EAGR	0.284	0.0398	0.0041
Common eider (*Somateria mollissima*)	COEI	0.572	0.1373	0.0118
Canvasback (*Aythya valisineria*)	CANV	0.501	0.0953	0.0090
Redhead (*Aythya americana*)	REDH	0.496	0.1010	0.0095

Models were for wing-propelled divers (penguin, alcids) with the wings removed and for foot-propelled divers (cormorant, loon, grebes, ducks) with the legs and feet removed.

fuselage (head and body trunk without propulsive limbs), we removed the legs and feet of foot-propelled divers (cormorants, loons, grebes, ducks) and the wings of wing-propelled divers (penguins, alcids). Lead plugs were inserted into holes drilled into the breast and leg muscles until each bird was neutrally buoyant and balanced (no pitching or rolling). In diving birds, greater pressure with increasing water depth will reduce air volumes in the respiratory system and plumage. The body will become thinner, decreasing drag to some extent as depth increases to the point where maximum compression of air spaces occurs (see Lovvorn and Jones, 1991; Lovvorn et al., 1999). However, such changes should have minimal effects when comparing frozen birds with models prepared from them at shallow depths in the tow tank or when comparing different species at the same depth.

Drag measurements

Drag was measured at the BC Research Ocean Engineering Center at the University of British Columbia, Vancouver, Canada. A carriage towed the models and frozen birds at specified speeds along a tank 3.7 m wide, 2.4 m deep and 61 m long.

In general, one of two methods has been used to suspend dead animals in a flow field for measuring drag: posts or struts that extend to the body from above or below (Pennycuick et al., 1988; Lovvorn et al., 1991) or stings that extend from the rear of the body (Hui, 1988; Bannasch, 1993; Bannasch et al., 1994; Lovvorn et al., 1999). Posts disrupt flow over the object, and the resulting 'interference drag' enhances measurements by an amount that is usually unknown (Tucker, 1990). Stings do not alter flow over the object. However, if force in only the backward direction is measured, both stings and posts require trial-and-error adjustment of the object's fixed angle during repeated runs to determine the angle of minimum drag. Otherwise, slight (and visually imperceptible) variations in the angle of attack can result in pitch or yaw (vertical or sideways

Table 2. *Body length including the bill and tail (L_b), body wetted surface area (A_{sw}) and maximum frontal area of individual frozen birds used for drag measurements*

Species	Species code	Length (m)	Surface area (m^2)	Frontal area (m^2)
Little penguin (*Eudyptula minor*)	LIPE	0.404	0.0758	0.0052
Common guillemot (*Uria aalge*)	COGU	0.482	0.0948	0.0084
Brünnich's guillemot (*Uria lomvia*)	BRGU	0.444	0.0969	0.0109
Tufted puffin (*Fratercula cirrhata*)	TUPU	0.395	0.0760	0.0077
Parakeet auklet (*Aethia psittacula*)	PAAU	0.270	0.0392	0.0038
Crested auklet (*Aethia cristatella*)	CRAU	0.241	0.0313	0.0035
Cassin's auklet (*Ptychoramphus aleuticus*)	CAAU	0.210	0.0274	0.0035
Whiskered auklet (*Aethia pymaea*)	WHAU	0.198	0.0219	0.0025
Least auklet (*Aethia pusilla*)	LEAU	0.173	0.0188	0.0021
Brandt's cormorant (*Phalacrocorax penicillatus*)	BRCO	0.760	0.1287	0.0162
King eider male (*Somateria spectabilis*)	KIEI male	0.565	0.1460	0.0162
King eider female (*Somateria spectabilis*)	KIEI female	0.495	0.1306	0.0154
Canvasback (*Aythya valisineria*)	CANV	0.531	0.0998	0.0100

Measurements are for wing-propelled divers (penguin, alcids) with the wings removed and for foot-propelled divers (cormorant, loon, grebes, ducks) with the legs and feet removed.

lift) that can enhance and even exceed the drag parallel to the flow field. Thus, without simultaneous measurements of forces in the backward, vertical and sideways directions, or trial-and-error adjustment of the sting's angle between runs on a progressively thawing animal, it is difficult to standardize measurements of minimum drag using posts or stings. Ideally, the suspension system should minimize disruption of flow over the body, while allowing the body to adjust automatically to its angle of minimum drag at different speeds.

To this end, we devised a harness using a drogue attached to and pulled behind the animal (Fig. 4). A vertical strut made of aluminum airfoil extrusion (5 cm deep by 2.5 cm wide) was bolted to the carriage superstructure midway across the tank and extended to 65 cm below the water surface. Nylon fishing line was attached to a force block mounted on the carriage above the strut, threaded around a pulley attached to the downward end of the strut, and extended horizontally backwards from the strut to the bird: thus, horizontal drag on the towed bird was measured as downward force on the block. The force block (model ST; Precision Transducers, Aukland, New Zealand) had a capacity of 50 kg force (490 N). The signal from the block was sampled at 50 Hz, processed by a signal conditioner (model DBK 16; IOtech, Cleveland, Ohio, USA) and archived on a personal computer.

After passing around the pulley at the bottom of the strut, the fishing line (20 kg test, 0.66 mm thick) extended horizontally backwards for 3.5 m, where it clipped to four 40 cm pieces of line that, in turn, were tied at four equidistant points around a polyvinylchloride (PVC) ring (6 cm outside diameter, 4 mm thick) (Fig. 4). Another four 40 cm pieces of line attached at these same points on the PVC ring ran backwards to clip onto small rings (4–5 mm in diameter) mounted at the top, bottom and either side of the bird's head. This four-point harness with the PVC ring was quite effective at preventing the bird from veering off course at all but the highest speeds. Another four lines attached at the top, bottom and either side of the rear of the trunk of the bird extended approximately 30 cm back to another clip at the end of a single line 2.6 m long that, in turn, clipped to an array of six 70 cm lines that attached at equal intervals around the circular forward opening of the drogue (Fig. 4).

Two drogues were used. Both were made of 3 mil Mylar (76 μm thick) folded into a tube and taped at the seam (3M brand 9576 double-sided tape with acrylic adhesive lasted under these conditions, while other tapes we tried did not).

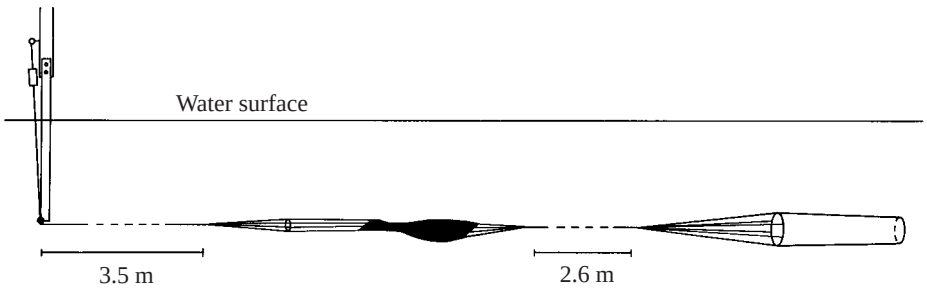

Fig. 4. The harness and drogue system used in drag measurements to avoid altering the flow over the body or the angle of attack by struts or stings.

Both drogues were 60 cm long and circular in cross section, with the area of the rear opening approximately 40 % smaller than that of the front opening. The front and rear openings were made rigid by taping a circle of aluminum welding rod (4 mm thick) inside the openings (3M 838 Tedlar weather-resistant tape). For most models and frozen birds, we used a drogue with front and rear diameters of 12 and 9 cm, respectively. For the eider model and the frozen eiders, guillemots, puffin, cormorant, penguin and canvasback (see Table 2), we used a drogue with front and rear diameters of 15 and 11.5 cm. The drag of the drogues was great enough to keep the birds horizontal during runs without a post or sting. The absence of a rigid attachment avoided interference with flow around the birds and allowed the birds to adjust automatically to their attack attitude of minimum drag.

At the start of a run, the bird and droque were held out by hand horizontally behind the strut at the depth of the pulley and were released when the carriage accelerated from its stationary position. Starting at 0.4 m s^{-1}, runs were made at successive speed increments of 0.3 m s^{-1} up to a maximum of 4.3 m s^{-1} or until the bird became unstable. If a frozen bird started to thaw, it was placed in a cooler over dry ice until refrozen. The drag of the towing assembly and drogue without a bird attached was subtracted from the drag with the bird included to yield the drag of the bird alone.

We calculated Reynolds numbers (*Re*) for the models and frozen birds with body length L_b (m) (including bill and tail) at each speed U (m s^{-1}) as $Re=UL_b/\nu$, where ν is the kinematic viscosity of fresh water at 20 °C (1.0037×10^{-6} m^2 s^{-1}). Drag coefficients (C_D) were calculated as $C_D=2D/\rho A_{sw}U^2$, where D is drag (in N), ρ is the density of fresh water at 20 °C (998.1 kg m^{-3}) and A_{sw} is the wetted surface area (m^2) of the bird or model.

Theoretically, drag is related only to the square of speed, but we included higher-order terms to fit the empirical curves exactly and thereby capture subtle effects of body shape. By analogy, according to the 'mouse-to-elephant curve', metabolic rate is related to body mass to the power 0.75; however, individual species often show meaningful deviations from this curve, which was developed over a very wide range of body mass. Moreover, we have found that small errors in regression curves fitted to drag data can cause significant changes in C_D/Re values calculated from those curves. In particular, a second-order drag/speed curve (as called for by theory) will curve up slightly at low speeds. However, this small deviation can cause substantial overestimates of C_D at low *Re*, making the C_D/Re curve resemble that for a cylinder rather than a streamlined body (Vogel, 1994). Patterns of C_D *versus* *Re* can also vary appreciably depending on the parameters used to calculate them, including the temperature and the salinity of the water (which affect ρ and ν), and especially body length (including or not including tails) and body area (wetted surface *versus* frontal). For example, the C_D/Re curve for cormorants is somewhat different (curves upwards) at high *Re* if their long tail is not included in the body length used to calculate *Re*. If another worker used a different method from ours to measure wetted surface area, the C_D/Re curves might also differ. We provide the parameters needed to calculate C_D and *Re* from our data in Tables 1, 2. However, by using the fitted drag/speed equations (Table 3), other authors can vary the parameters for calculating C_D or *Re* according to particular conditions and analyses.

To fit polynomial equations to the data for each specimen (model or frozen bird), we used a combination of multiple regression and inspection of the resulting plots. We first calculated coefficients of multiple determination (R^2) for all possible subsets of the independent variable (speed) raised to powers up to 5 (α for entry into the model was 0.15; SAS Institute, 1987). Plots of observed *versus* predicted values for equations with the highest R^2 values were then visually inspected to select the equation showing the fewest deviations. Note that the regression routine was used only as a curve-fitting method to fit a polynomial equation to data for a single specimen (model or frozen bird); the resulting equations did not represent a population of different specimens for each species. Thus, there was no population variance for each curve,

Table 3. *Equations for drag* D *(in N) versus speed* U *(m s^{-1}) of individual frozen specimens of each species*

Species	Species code	Equation
Little penguin	LIPE	$D=-0.255+1.67U-0.387U^2+0.228U^3$
Common guillemot	COGU	$D=2.25-3.78U+5.02U^2-1.40U^3+0.0494U^5$
Brünnich's guillemot	BRGU	$D=1.08+2.55U^2-1.38U^3+0.276U^4$
Tufted puffin	TUPU	$D=0.230+3.56U^2-2.05U^3+0.394U^4$
Parakeet auklet	PAAU	$D=-1.13+6.16U-8.12U^2+5.25U^3-1.51U^4+0.163U^5$
Crested auklet	CRAU	$D=-0.271+2.34U-3.16U^2+2.36U^3-0.764U^4+0.0931U^5$
Cassin's auklet	CAAU	$D=-0.206+1.28U-0.267U^2+0.0914U^3$
Whiskered auklet	WHAU	$D=-1.40+4.77U-5.00U^2+3.03U^3-0.805U^4+0.0798U^5$
Least auklet	LEAU	$D=0.174+0.387U-0.0126U^2+0.0154U^4$
Brandt's cormorant	BRCO	$D=1.21-1.74U+3.76U^2-1.38U^3+0.213U^4$
King eider male	KIEI male	$D=0.457+1.33U+0.944U^2$
King eider female	KIEI female	$D=-0.530+3.03U-3.10U^2+3.73U^3-1.54U^4+0.226U^5$
Canvasback	CANV	$D=0.703-0.854U+2.65U^2-0.801U^3+0.0899U^4$

Higher-order terms represent details of shape effects on drag at different speeds (see text).

so that statistical comparisons among curves for different species were inappropriate.

Results

Effects of feathers

Curves of drag *versus* speed and C_D *versus Re* were compared between the models and individual frozen specimens selected from those used to develop the models (Fig. 5). The drag of frozen birds was 2–6 times higher than that of the models. Differences tended to be greater for long-necked birds that swim with their neck extended (CANV, BRCO) than for wing-propelled divers that swim with their neck retracted (LIPE, COGU, CAAU). The model for the Cassin's auklet (CAAU) apparently became unstable at speeds greater than 3 m s^{-1}, resulting in a rapid increase in drag (Fig. 5). For long-necked species, the C_D/*Re* plots for both model and frozen birds resembled those for smooth streamlined shapes (Vogel, 1994). For birds that swim with a retracted neck, the C_D/*Re* plots for the models also resembled those for smooth streamlined shapes, whereas those for the frozen birds resembled those for rough streamlined shapes. Feathers had greater effects on the magnitude of drag curves than on their general shape.

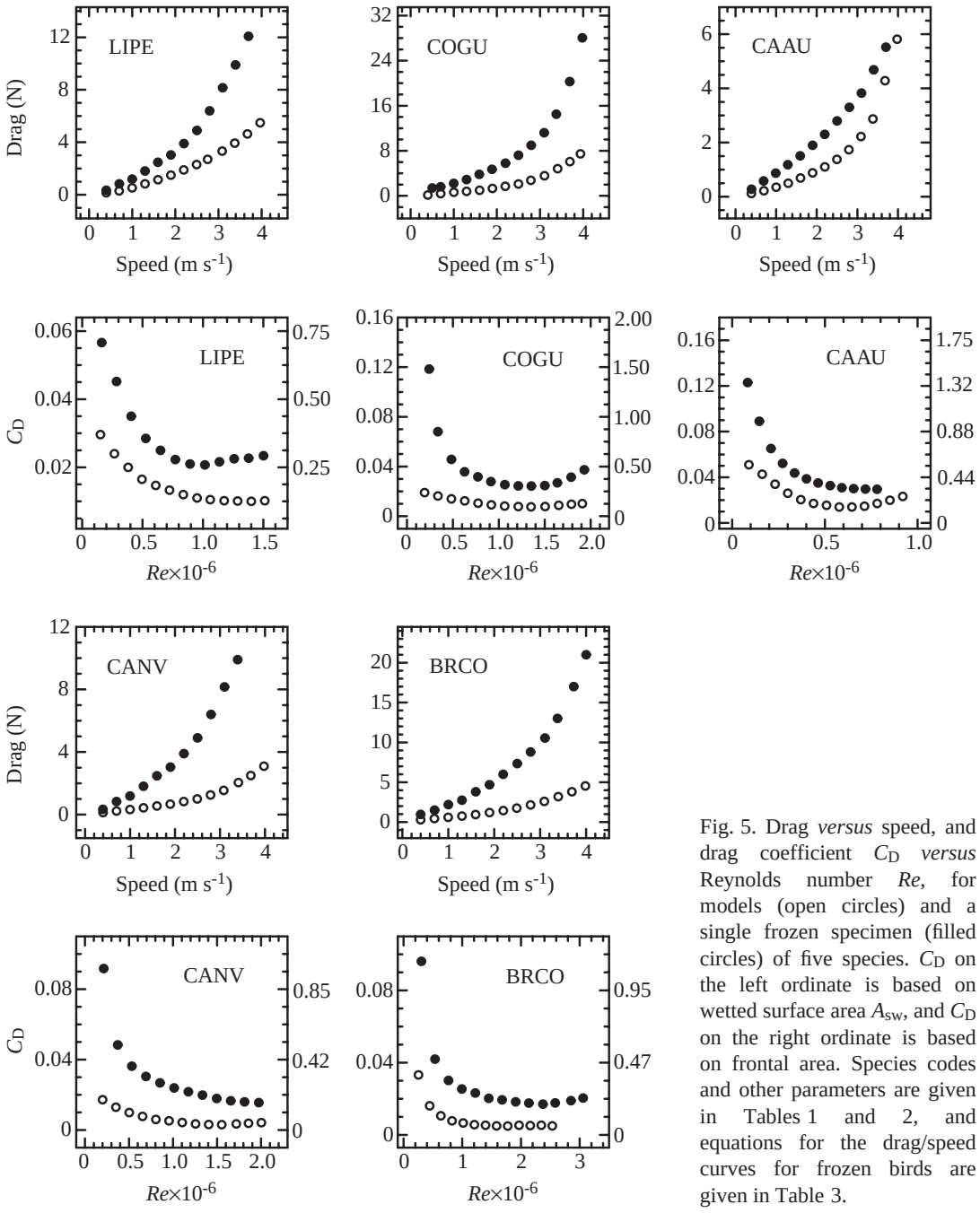

Fig. 5. Drag *versus* speed, and drag coefficient C_D *versus* Reynolds number *Re*, for models (open circles) and a single frozen specimen (filled circles) of five species. C_D on the left ordinate is based on wetted surface area A_{sw}, and C_D on the right ordinate is based on frontal area. Species codes and other parameters are given in Tables 1 and 2, and equations for the drag/speed curves for frozen birds are given in Table 3.

Effects of shape independently of feathers

Birds with different propulsive and foraging modes generally have different shapes, and we evaluated the effects of these differences on drag at steady speeds. We divided the birds into four categories: wing-propelled penguins that do not fly in air, wing-propelled alcids (murres, puffins, auklets) that do fly in air, foot-propelled pursuers (cormorants, loons, grebes) and foot-propelled benthivores (ducks) (Fig. 3).

Although penguins are often considered to have the least drag of possible bird shapes (see Nachtigall and Bilo, 1980; Bannasch, 1993), the body fuselage of the model common guillemot (common murre) had a lower C_D at all *Re* values than did the little penguin model (i.e. lower drag corrected for body surface area and length) (Fig. 6A). The drag of model rhinoceros and Cassin's auklets increased abruptly and dramatically at intermediate *Re* values corresponding to mean speeds much higher than those at which they normally swim (probably 1–1.5 m s^{-1}; J. R. Lovvorn, unpublished observations); this difference from the penguin and guillemot occurred without the effects of feathers. Models of foot-propelled pursuers (Fig. 6B), which all swim with their neck extended, generally had lower C_D values than the wing-propelled birds, especially at high *Re* (except for the red-throated loon). The eared grebe model had the lowest drag of all species studied. Although the common eider model had a C_D value similar to those of wing-propelled divers at low *Re*, it had a lower C_D at high *Re* (Fig. 6C). Models of the other foot-propelled benthivores (canvasback and redhead ducks) had C_D values even lower than those of foot-propelled pursuers. These data indicate important and consistent differences in drag patterns among species that result mainly from differences in shape.

Effects of size and shape for feathered birds

General differences among propulsive modes and body shapes (Fig. 3) were evident for a wider range of frozen birds. The C_D/*Re* curves were similar among large wing-propelled divers (Fig. 7A), being higher than those for foot-propelled divers at high *Re* (Fig. 7C). Although the C_D of the model penguin was higher than that of the model guillemot (Fig. 6A), the pattern was reversed for the frozen birds (Fig. 7A); this difference might have resulted from the unique structure of penguin feathers (Stahel et al., 1987), which are less likely to flutter. Also, although the model common eider had a much higher drag and C_D than models of other foot-propelled benthivores (Fig. 6C), among frozen birds the C_D of the male king eider was quite similar to that of the Brandt's cormorant, and that of the female king eider was even lower at all but the highest *Re* values.

Wing-propelled small auklets of apparently similar body shape but differing size (Table 2) had C_D/*Re* curves of similar shape but different magnitude, and these patterns did not correspond consistently with body size (Fig. 7B). For example, the C_D/*Re* curves for the parakeet and crested auklets were almost the same, the curves for Cassin's and whiskered auklets seemed to correspond with body size, and the curve for least auklets seemed to be unrelated to body size.

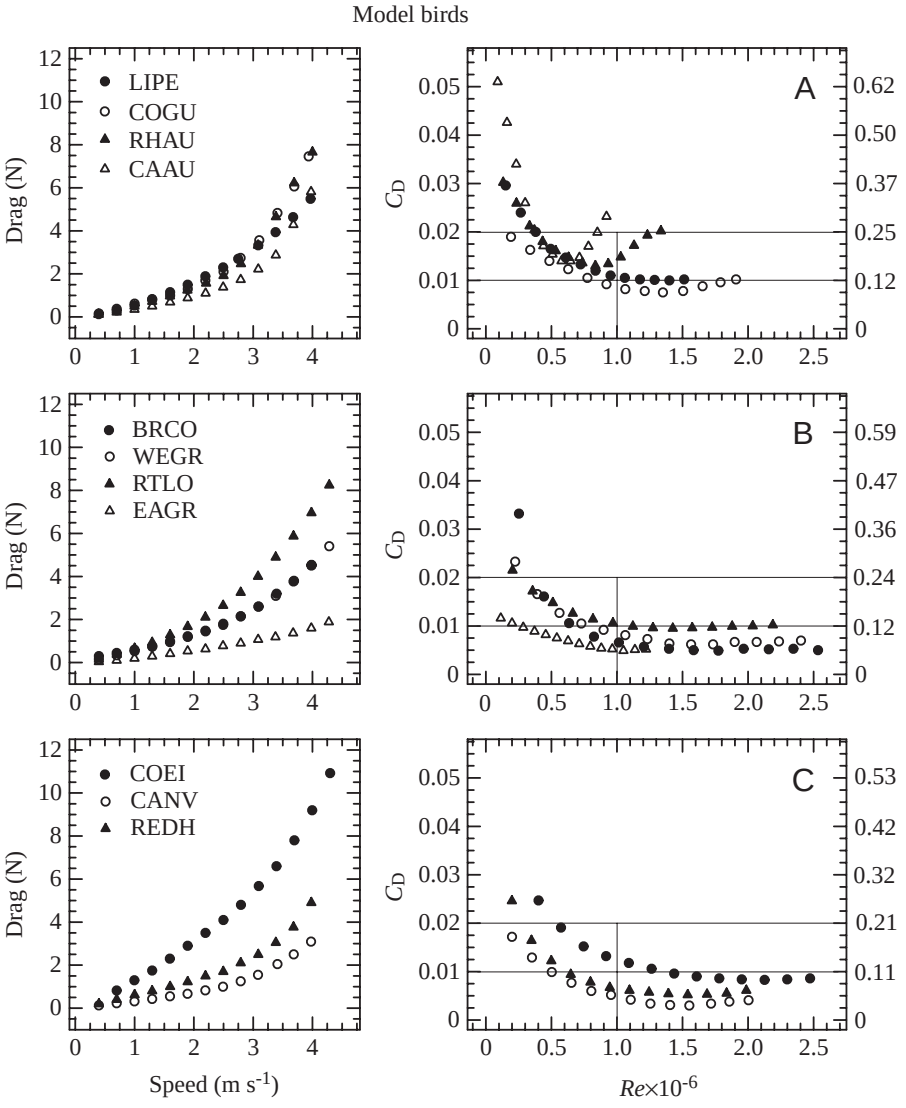

Fig. 6. Drag *versus* speed, and drag coefficient C_D *versus* Reynolds number *Re*, for models of (A) wing-propelled divers, (B) foot-propelled pursuers and (C) foot-propelled benthivores. C_D on the left ordinate is based on wetted surface area A_{sw}, and C_D on the right ordinate is based on frontal area. Body shapes are given in Fig. 3, and species codes and other parameters are given in Table 1.

For large wing-propelled *versus* foot-propelled divers, the C_D of the little penguin (and of Brünnich's guillemot at low speeds) was lower than that of long-necked birds at lower *Re*, whereas this pattern was reversed at higher *Re* (Fig. 8). Corresponding speeds at which this transition occurred ($Re \approx 1.3\times10^{-6}$) were approximately 3.1 m s^{-1} for the penguin and guillemot, but only 1.6 m s^{-1} for the cormorant and 2.2 m s^{-1} for the male king eider, whose curve was very similar to that of the cormorant (cf. Fig. 7C). Note that, in our frozen Brünnich's guillemot (thick-billed murre), the head was more retracted than in the frozen common guillemot and others scanned to create the common guillemot model (Figs 2, 3).

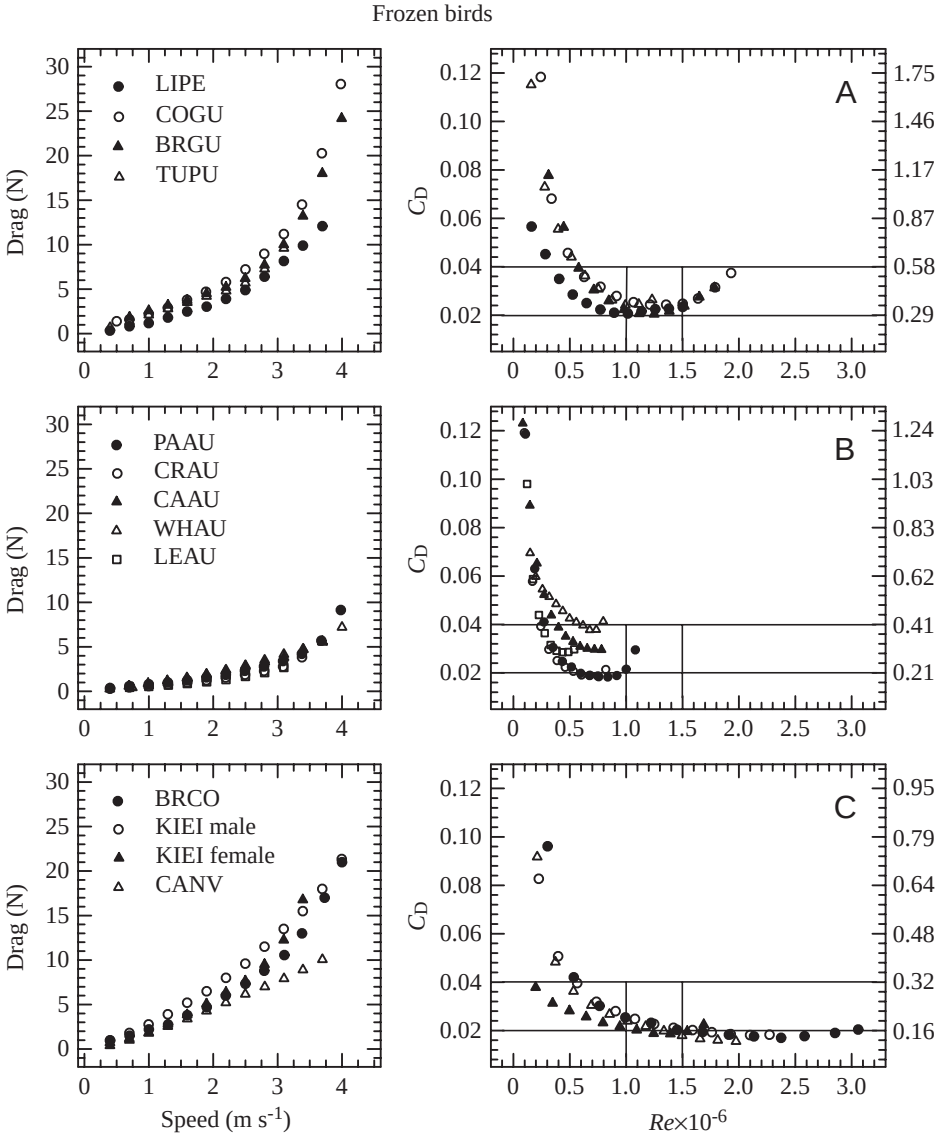

Fig. 7. Drag *versus* speed, and drag coefficient C_D *versus* Reynolds number *Re*, for single frozen specimens of (A) wing-propelled divers, (B) wing-propelled auklets and (C) foot-propelled divers. C_D on the left ordinate is based on wetted surface area A_{sw}, and C_D on the right ordinate is based on frontal area. Species codes and other parameters are given in Table 2, and equations for drag curves are given in Table 3.

Discussion

Our data indicate that the roughness and vibration of feathers can increase the drag of frozen birds by two- to sixfold over that of cast models or other featherless bird shapes. Thus, the effects of feathers must be considered in drag measurements and in the resulting estimates of locomotor cost. The magnitude of the 'feather factor' varied with both speed and species, with apparently greater effects in foot-propelled divers that swim with their neck extended (cf. Figs 3 and 5). In our study, this difference probably resulted from the fact that the wings of foot-propelled divers, which are held against the body during swimming, were not removed and remained part of the body fuselage. The longer wing feathers (including flight feathers, scapulars and tertials) probably vibrated more than the shorter contour feathers alone in wing-propelled divers whose wings were removed. Also, the unique structure of penguin feathers, which probably reduces vibration and fluttering, apparently decreased the drag of the penguin below that expected on the basis of shape alone (compare the C_D/Re curves of LIPE and COGU in Figs 6A and 7A). The anomalous, rapid increase in drag at high speeds of the model Cassin's auklet (Fig. 5) is probably irrelevant because the increase occurred at speeds far greater than the mean speed that this species normally achieves (probably approximately 1.2 m s^{-1}; J. R. Lovvorn, unpublished observations)

Pennycuick et al. (Pennycuick et al., 1996) suggested that the drag of frozen birds in air is greater than for live birds because their feathers flutter unrealistically, amplify turbulence and enhance flow separation. Hui (Hui, 1983) expressed similar concerns in comparing the underwater drag of a penguin preserved in formalin with that of a cast model of the same individual. Muscles at the bases of the feather shafts probably affect the flexibility of individual feathers and of the plumage surface as a whole; the loss of this control might enhance the drag of frozen birds, especially at higher speeds. However, the feathers of free-living birds often flutter noticeably in air, and it is likely that appreciable flutter effects occur during swimming by living birds. Except for the rhinoceros and Cassin's auklet models (Figs 5, 6), the shapes of the curves

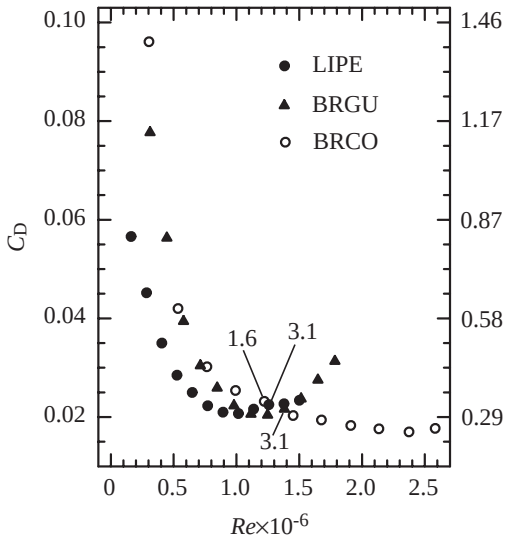

Fig. 8. Drag coefficient C_D *versus* Reynolds number *Re* for single frozen specimens of two wing-propelled divers that swim with their neck retracted (LIPE and BRGU) and a foot-propelled diver that swims with its long neck extended (BRCO). Species codes are in given Table 2. C_D on the left ordinate is based on wetted surface area A_{sw}, and C_D on the right ordinate is based on frontal area. Speeds (in $m\,s^{-1}$) corresponding to *Re* where the BRCO curve crosses the curves for the wing-propelled species are annotated. The C_D/Re curve for the foot-propelled male KIEI is very similar to that for the BRCO (cf. Fig. 7C) and crosses the C_D/Re curves for these wing-propelled species at a corresponding speed of approximately $2.2\,m\,s^{-1}$.

indicate that the boundary layer did not separate for any species except at the highest speeds tested. In fact, the roughness and perhaps flutter of the feathers might have delayed separation in frozen birds as opposed to these smooth models by ensuring a more stable, fully turbulent boundary layer.

Differences between C_D/Re plots for frozen *versus* model birds of the same species (Fig. 5) suggest that feathers are important in creating fully turbulent flow at all speeds. Bannasch (Bannasch, 1993) found that the C_D/Re plot for a smooth body of revolution was the same as plots for cast penguin models if turbulence in the boundary layer was induced by a wire around the front of the axisymmetric body. He concluded that either the shape or the surface roughness of penguin heads caused the transition to a turbulent boundary layer and that flow did not separate along the entire body. Similar arguments have been made for a variety of fast-swimming fish with a long rostrum, in particular because of the alternating concave and convex profiles at the base of the rostrum and the crest of the head that promote turbulence (Aleyev, 1977; Bandyopadhyay, 1989). In our study, the fact that the C_D/Re plots differed somewhat between smooth and feathered versions of the same shapes (Fig. 5) suggests that feathers play a role in addition to head shape in causing the transition to a turbulent boundary layer near the front of the body. Feathers appeared to have greater effects on the magnitude of drag than on the relative shapes of the drag and C_D/Re plots among species.

Differences in body shape among bird species had strong effects on patterns of change in drag with speed. In the case of auklets, seemingly minor variations in shape caused fairly dramatic changes in C_D (Fig. 7B), and these shape differences were not consistently related to size (e.g. in the least auklet; Table 2). Because such differences were not apparent without drag measurements, extrapolation of dimensionless C_D/Re curves among 'similar' species must be performed with caution.

For larger birds, C_D/Re curves varied rather consistently between wing-propelled divers with short or retracted necks *versus* foot-propelled divers that swim with their neck extended. This pattern held generally for model birds (Fig. 6) but was more striking in frozen birds (Figs 7, 8). For example, although C_D of the cormorant was much higher than that of the penguin and sometimes that of the guillemot at $Re<1.3\times10^{-6}$, above that point C_D of the cormorant (and of the male king eider with a very similar curve) was substantially lower. On the basis of the speeds corresponding to these *Re* values (Fig. 8), the long extended neck of cormorants (Fig. 3) is a disadvantage at speeds below $1.6\,m\,s^{-1}$, but an advantage at higher speeds. For male king eiders, this transition occurs at approximately $2.2\,m\,s^{-1}$. Cormorants should benefit from their shape both at higher mean speeds and at most instantaneous speeds during strokes (J. R. Lovvorn, A. Kato, Y. Watanuki and Y. Naito, unpublished results), whereas king eiders should benefit only at the higher instantaneous speeds. Because both the mean and instantaneous speeds of little penguins and guillemots seldom exceed $3.1\,m\,s^{-1}$ (Clark and Bemis, 1979; Lovvorn, 2001; Lovvorn et al., 1999), they should always benefit from having short or retracted necks (Fig. 3).

In considering differences among species in drag at steady speeds, it must be remembered that birds do not actually swim at constant mean speeds, but rather at a wide range of instantaneous speeds throughout oscillatory strokes (Lovvorn et al., 1991; Lovvorn et al., 1999). For example, because little or no thrust is generated during the upstroke in foot propulsion, whereas wing propulsion allows thrust to be produced during both the upstroke and downstroke, foot-propelled birds must have higher speeds during a smaller fraction of the stroke to maintain the same mean speed. Drag increases rapidly with increasing speed, so the costs of swimming are strongly influenced by drag on the body fuselage at high instantaneous speeds (Lovvorn, 2001). Thus, the lower fuselage drag of foot-propelled divers at high steady speeds might mitigate the higher drag of foot propulsion, but such effects must be placed in the context of drag at a range of instantaneous speeds during oscillatory strokes. We are exploring these effects in modeling studies of accelerational stroking (J. R. Lovvorn and G. A. Liggins, unpublished results).

We thank G. V. Byrd, P. Dann, M. B. Decker, D. A. Dorado, G. L. Hunt, F. P. Kehoe, A. L. Sowls, R. Stephenson and J. Williams for obtaining bird specimens and D. R. Jones for initial financial support. G. N. Stensgaard of the BC Research Ocean Engineering Center allowed use of the drag

tank, and A. Akinturk, A. I. Field and M. MacKinnon helped with drag measurements. This research was supported by US National Science Foundation grant OPP-9813979 to J.R.L.

References

Aleyev, Y. G. (1977). *Nekton*. The Hague: Dr W. Junk Publishers.

Bandyopadhyay, P. R. (1989). Viscous drag reduction of a nose body. *Am. Inst. Aeronaut. Astronaut. J.* **27**, 274–282.

Bannasch, R. (1993). Drag minimisation on bodies of revolution in nature and engineering. In *Proceedings of the International Airship Conference*, pp. 79–87. Universität Stuttgart, Germany.

Bannasch, R. (1995). Hydrodynamics of penguins – an experimental approach. In *The Penguins* (ed. P. Dann, I. Norman and P. Reilly), pp. 141–176. Chipping Norton, NSW, Australia: Surrey Beatty & Sons.

Bannasch, R., Wilson, R. P. and Culik, B. (1994). Hydrodynamic aspects of design and attachment of a back-mounted device in penguins. *J. Exp. Biol.* **194**, 83–96.

Bilo, D. and Nachtigall, W. (1980). A simple method to determine drag coefficients in aquatic mammals. *J. Exp. Biol.* **87**, 357–359.

Clark, B. D. and Bemis, W. (1979). Kinematics of swimming of penguins at the Detroit Zoo. *J. Zool., Lond.* **188**, 411–428.

Faugeras, O. (1996). *Three-dimensional Computer Vision*. Cambridge, MA: Massachusetts Institute of Technology Press.

Feldkamp, S. D. (1987). Swimming in the California sea lion: morphometrics, drag and energetics. *J. Exp. Biol.* **131**, 117–135.

Fish, F. E. (1984). Mechanics, power output and efficiency of the swimming muskrat (*Ondatra zibethicus*). *J. Exp. Biol.* **110**, 183–201.

Fu, K. S., Gonzalez, R. C. and Lee, C. S. G. (1987). *Robotics: Control, Sensing, Vision and Intelligence*. New York: McGraw-Hill.

Hoerner, S. F. (1965). *Fluid-dynamic Drag*. Midland Park, NJ: published by the author.

Hui, C. A. (1983). Swimming in penguins. PhD thesis, University of California, Los Angeles, USA.

Hui, C. A. (1988). Penguin swimming. I. Hydrodynamics. *Physiol. Zool.* **61**, 333–343.

Kooyman, G. L. (1989). *Diverse Divers*. Berlin: Springer-Verlag.

Lovvorn, J. R. (2001). Upstroke thrust, drag effects, and stroke-glide cycles in wing-propelled swimming by birds. *Am. Zool.* (in press).

Lovvorn, J. R., Croll, D. A. and Liggins, G. A. (1999). Mechanical *versus* physiological determinants of swimming speed in diving Brünnich's guillemots. *J. Exp. Biol.* **202**, 1741–1752.

Lovvorn, J. R. and Jones, D. R. (1991). Effects of body size, body fat and change in pressure with depth on buoyancy and costs of diving in ducks (*Aythya* spp.). *Can. J. Zool.* **69**, 2879–2887.

Lovvorn, J. R., Jones, D. R. and Blake, R. W. (1991). Mechanics of underwater locomotion in diving ducks: drag, buoyancy and acceleration in a size gradient of species. *J. Exp. Biol.* **159**, 89–108.

Nachtigall, W. and Bilo, D. (1980). Strömungsanpassung des Pinguins beim schwimmen unter Wasser. *J. Comp. Physiol.* A **137**, 17–26.

Oehme, H. and Bannasch, R. (1989). Energetics of locomotion in penguins. In *Energy Transformations in Cells and Organisms* (ed. W. Wieser and E. Gnaiger), pp. 230–240. New York: Thieme.

Pennycuick, C. J. (1989). *Bird Flight Performance*. Oxford: Oxford University Press.

Pennycuick, C. J., Klaassen, M., Kvist, A. and Lindstrom, A. (1996). Wingbeat frequency and the body drag anomaly: wind-tunnel observations on a thrush nightingale (*Luscinia luscinia*) and a teal (*Anas crecca*). *J. Exp. Biol.* **199**, 2757–2765.

Pennycuick, C. J., Obrecht, H. H. and Fuller, M. R. (1988). Empirical estimates of body drag of large waterfowl and raptors. *J. Exp. Biol.* **135**, 253–264.

Purves, P. E., Dudok van Heel, W. H. and Jonk, A. (1975). Locomotion in dolphins. I. Hydrodynamic experiments on a model of the bottle-nosed dolphin, *Tursiops truncatus* (Mont.). *Aquat. Mammals* **3**, 5–31.

SAS Institute (1987). *SAS/STAT Guide for Personal Computers*, Version 6 edition. Cary, NC: SAS Institute.

Skrovan, R. C., Williams, T. M., Berry, P. S., Moore, P. W. and Davis, R. W. (1999). The diving physiology of bottlenose dolphins (*Tursiops truncatus*). II. Bioemechanics and changes in buoyancy at depth. *J. Exp. Biol.* **202**, 2749–2761.

Spring, L. (1971). A comparison of functional and morphological adaptations in the common murre (*Uria aalge*) and thick-billed murre (*Uria lomvia*). *Condor* **73**, 1–27.

Stahel, C., Gales, R. and Burrell, J. (1987). *Little Penguin*. Kensington: New South Wales University Press.

Stelle, L. L., Blake, R. W. and Trites, A. W. (2000). Hydrodynamic drag in Steller sea lions (*Eumetopias jubatus*). *J. Exp. Biol.* **203**, 1915–1923.

Tucker, V. A. (1990). Body drag, feather drag and interference drag of the mounting strut in a peregrine falcon, *Falco peregrinus*. *J. Exp. Biol.* **149**, 449–468.

Vogel, S. (1994). *Life in Moving Fluids*. Second edition. Princeton, NJ: Princeton University Press.

Webb, P. W. (1975). Hydrodynamics and energetics of fish propulsion. *Bull. Fish. Res. Bd Can.* **190**, 159 pp.

Williams, T. M. (1983). Locomotion in the North American mink, a semi-aquatic mammal. I. Swimming energetics and body drag. *J. Exp. Biol.* **103**, 155–168.

Williams, T. M. (1989). Swimming by sea otters: adaptations for low energetic cost locomotion. *J. Comp. Physiol.* A **164**, 815–824.

Williams, T. M. and Kooyman, G. L. (1985). Swimming performance and hydrodynamic characteristics of harbor seals *Phoca vitulina*. *Physiol. Zool.* **58**, 576–589.